applied sciences

MDPI

Article

Simulation of Different Control Strategies of a Three-Phase Induction Motor Coupled to a Real Decanter Centrifuge for Olive Oil Extraction Focusing on Energy Saving

Orkhan Mammadov, Giuseppe Altieri *, Francesco Genovese, Sabina Laveglia, Attilio Matera, Mahdi Rashvand, Luciano Scarano and Giovanni Carlo Di Renzo

School of Agricultural Forest Food and Environmental Sciences, University of Basilicata, 85100 Potenza, Italy; orkhan.mammadov@unibas.it (O.M.); francesco.genovese@unibas.it (F.G.); sabina.laveglia@unibas.it (S.L.); attilio.matera@unibas.it (A.M.); mahdi.rashvand@unibas.it (M.R.); luciano.scarano@unibas.it (L.S.); giovanni.direnzo@unibas.it (G.C.D.R.)

* Correspondence: giuseppe.altieri@unibas.it

Abstract: This study presents the analysis and modeling of the optimal connection between an asynchronous three-phase electrical induction motor and a horizontal centrifuge used in olive oil extraction. The simulation, carried out using the well-established Simscape Electrical by Matlab R2024a, offers the advantage of reducing the purchasing cost of the electronic drivers and electric motors to be tested. Different connection cases among the electronic motor driver, the electric motor, and the horizontal centrifuge were examined. The findings indicate that the oversizing of the electric motor is required to increase the machine efficiency and to reduce the overall specific energy consumption; however, the asymptotic behavior of the specific energy consumption, being related to the motor power, places a limit on the motor oversizing. Indeed, raising the motor power reduces the specific energy consumption; however, this effect can be unimportant if considering the higher cost involved in purchasing both the electrical motor and the electronic motor driver. The results show that an overall percentage saving of specific energy consumption of 3.1% and 4.0% can be achieved with a slight (7.5 kW) and a medium (11 kW) oversizing of the electric motor, respectively.

Keywords: induction three-phase asynchronous motor; variable-frequency drive; Simulink modeling; efficiency

Citation: Mammadov, O.; Altieri, G.; Genovese, F.; Laveglia, S.; Matera, A.; Rashvand, M.; Scarano, L.; Di Renzo, G.C. Simulation of Different Control Strategies of a Three-Phase Induction Motor Coupled to a Real Decanter Centrifuge for Olive Oil Extraction Focusing on Energy Saving. *Appl. Sci.* **2024**, *14*, 6624. https://doi.org/10.3390/app14156624

Academic Editor: José Miguel Molina Martínez

Received: 16 June 2024
Revised: 24 July 2024
Accepted: 25 July 2024
Published: 29 July 2024

1. Introduction

The electrical motor is an important device that converts electrical energy into mechanical energy, which is necessary for daily life and economic activity. Beyond its financial worth, its applications are widely used and have a substantial impact on technological advancement and industrial development [1]. Low-voltage motor and drive sales worldwide were estimated to be worth USD 23.8 billion in 2021, up 4.1% from 2017 [2]. Electric motors currently use more than 7000 TWh annually. Studies demonstrate a significant potential for energy savings by improving motor efficiency. High efficiency standards are required since electric motors account for 80% of global electricity use, despite global attempts to reduce the greenhouse effect [3]. By 2030, that consumption and the associated CO_2 emissions might increase by about 90%, if appropriate action is not taken [2].

All the components need to be appropriately sized to function at an optimal operating point. This optimal point is determined by the sizing of the components and their suitability for the specific application. Among the most common misapplications, motor oversizing is highly problematic and hard to correct [4]. Excessive oversizing needs to be prevented, as it causes the equipment to operate at an inefficient operating point. However, motor oversizing is still a common practice in the industry. Power losses when a motor is not operating at its optimum operating point are higher with respect to those of a less efficient

motor but operating in its rated efficiency range [2]. The optimal operating load for motors is 75% of their rated load or higher. Due to their affordability, dependability, and low maintenance requirements, induction motors account for over 80% of all electric motors and also do not need a starting device, because they start themselves.

To maximize energy savings, the power output of motors must be accurately matched to the mechanical load they will drive. Most induction motors are designed to operate efficiently from 50% to 100% of their full load, with peak efficiency typically around 75% of full load. Motors operating below 75% generally decrease their efficiency. Therefore, oversizing motors can lead to increased energy consumption costs [5]. Auxiliaries, transmission, motor, motor control, power supply, and mechanical load are some of the parts of a motor-based application.

There are two methods for improving such systems' energy efficiency.

(1) Component approach method: This method entails creating Minimum Efficiency Performance Standards (MEPSs) for important components and making sure they all fulfill minimal energy efficiency standards.
(2) System approach method: This method promotes higher energy savings and a better optimization than the component approach by taking into account the full application to achieve overall system efficiency.

When evaluating a motor-based application, the actual efficiency is determined by how well the equipment components match the application requirements. This includes taking into account variables such as the transmission operating point, motor operating point (both speed and torque), motor control system (starter or variable speed drive), and mechanical equipment operating point.

Modern applications often require variable speeds, even though most motors are designed for a fixed speed and output. Leonard Abbott III [6] noted that full-load operation is unnecessary in about 25% of induction motor applications. Motors typically run at 100% speed only for short durations, making speed regulation crucial.

Variable-frequency drive (VFD) addresses this need by converting a fixed voltage and frequency input to a variable frequency and voltage output, thus effectively managing the motor speed or torque, enhancing automation, and saving energy. VFDs are used in a wide range of applications, including electric cars, pumps, elevators, fans, robotics, and air conditioning [1]. Total low-voltage VFD revenues were estimated at approximately USD 11.5 billion.

VFDs allow applications to use a much higher starting torque and reduced energy consumption once the application is operating. This feature is crucial, due to the low starting torque of high-efficiency systems.

Research has been focused on the study of the interaction between the electric motor and the variable frequency driver and between the electric motor and the operated device.

Saidur et al. [7] reported that VFD systems can save about 15–40% energy and extend equipment lifespans by enabling gentle start-up and shutdown.

Wang et al. [8] reported that in their experiments, VFDs significantly reduced system input power by 85% at a 50% rated frequency and increased the power factor to 0.95 at a 95% rated frequency, with a voltage total harmonic distortion (THD) always less than 1%.

Ekren et al. [9] investigated a variable-speed compressor refrigerator in both on/off and variable-speed modes, finding a 10% increase in exergy efficiency and a 14% increase in the coefficient of performance (COP) due to variable-speed operation.

Piedrahita-Velásquez et al. [10] demonstrated that VFD saved 15% energy compared to the on/off mode in tests with household refrigeration systems using a variable-speed compressor.

Yilmaz et al. [11] reported that in tests on VFDs in compressors for ship cold storage refrigeration, the COP improved by 13.9% as the compressor frequency decreased.

Cini et al. [12] evaluated the electric energy consumption of small to medium-sized Tuscan olive oil mills, taking into account all equipment and process steps, including pumps and fans. Centrifugal extractors and crushers are examples of process equipment

driven by electrical motors, and their energy consumption during the production campaign can be substantial, particularly when the decanter centrifuges operate for extended periods of time. In this case, to ensure rapid decanter operation, the electrical motors are sometimes oversized, resulting in suboptimal efficiency.

Tamborrino et al. [13] proposed a model to study the energy consumption of a decanter equipped with an electromechanical recovery system (i.e., regenerative braking), also reporting how the use of the installed power varied from 20% to 40%, resulting in a sub-utilization of the installed power and in a not-efficient energy utilization.

Leone et al. [14] created a model to study the energy requirement of a decanter centrifuge driven by VFDs and equipped with a regenerative braking recovery; the aim was to identify the energetic optimal conditions and their relation to the quality of the product.

Therefore, it is very difficult to operate the motor at its maximum efficiency, because different restraints have to be considered (e.g., the time to bring the device to the operating speed, different and variable motor loads, and the behavior of the load with regard to the shaft speed); furthermore, a study analyzing the operating efficiency of a motor, while also taking into account the possibility of operating the motor at different speed using a gearbox and a variable-frequency driver, is lacking.

Some researchers demonstrated how variable-frequency drivers using the V/F operation reach a good efficiency when the motor is operated near the full load region [15], and, for this reason, the idea was to investigate the use of a gearbox to adapt the load to the motor's optimal torque, thus also adapting the efficiency curve of the three-phase electric motor.

Through simulations and experimental measurements, this study seeks to determine the existing relationship between the system's overall efficiency and an electronic-driven motor connected to a horizontal centrifuge, demonstrating, in addition, the applicability of simulation programs in engineering problems related to electric motors [16,17]. The simulation made it possible to test the system without the high cost of purchasing electric motors and variable-frequency drivers.

2. Materials and Methods

The machine used was a horizontal decanter centrifuge BABY-1 from "Pieralisi" available in the laboratory, with an operating throughput of 500 kg/h, coupled to an asynchronous three-phase induction motor (IM) by "ABB" with 5.5 kW of nominal mechanical power. The connection between the electric motor and horizontal centrifuge is established by pulleys and two toothed drive belts with a measured gearbox ratio of 1.7365.

A timetable, arising from a real olive oil mill, was used to simulate the activity period of the device constituted by motor + decanter (MD).

When considering the overall working time per day, from the timetable it arises that the MD is run unloaded for 6% of its daily operating time, while the MD is run loaded for the rest of the daily operating period (94%). We considered a 40-day working period, with increasing working hours per day at the start (first nine days) from 7 to 20 and decreasing working hours per day at the end (last seven days) from 20 to 7, with a plateau of 20 h per day in the middle (consisting of the remaining 24 days).

The results of the simulation have been used in conjunction with the previously described timetable over a 40-day campaign period.

Some assumptions have been made:

(a) The dilution ratio (i.e., the ratio between the mass of added lukewarm water and the mass of olive oil paste) is considered to be 0.2 (the normal dilution ratio for high-quality extra virgin olive oil extraction);
(b) The horizontal centrifuge full productive capacity is considered to be exactly equal to 500 kg/h.

From the operational timetable previously described, it arises that the overall processed product was 226,685 kg on 627 overall working hours, the time that the horizontal centrifuge

was run unloaded was 37.62 h, and the time that the horizontal centrifuge was run at full load was 589.38 h.

The final results considered are the following: the overall energy consumption per processed product unit mass (OSEC) expressed as kJ/kg; the overall specific energy wasted (i.e., the difference between the active power and the mechanical power at the motor shaft) per processed product unit mass (OSEW) arising from the wasted power considered as the overall (MD) centrifuge and electric motor wasted electrical power, expressed as kJ/kg; and, finally, the overall process efficiency (OPE) obtained by the following relation (OSEC-OSEW)/OSEC.

The relations are the following.

$$\text{OSEC} = (\text{ActivePower} \times \text{TimeDecanterLoaded} + \text{ActivePower} \times \text{TimeDecanterUnloaded})/\text{OverallProcessedProduct}$$

$$\text{OSEW} = (\text{WastedPower} \times \text{TimeDecanterLoaded} + \text{ActivePower} \times \text{TimeDecanterUnloaded})/\text{OverallProcessedProduct}$$

$$\text{OPE} = (\text{OSEC} - \text{OSEW})/\text{OSEC}$$

The configuration of the centrifuge coupled to a 5.5 kW electric motor, connected directly to the power line (DOL), was assumed as a reference for the comparison of subsequent simulations.

Table 1 presents the fundamental reference parameters obtained when connecting the MD machine with the M4 motor-connected DOL.

Table 1. Fundamental reference parameters as obtained for the horizontal centrifuge coupled to a 5.5 kW motor connected directly to the power line (DOL).

OSEC (kJ/kg)	OSEW (kJ/kg)	OPE
30.613	6.002	0.8039

Matlab R2024a Simulink software (using Simscape Electrical, formerly SimPowerSystems) from MathWorks was used to simulate the physical system; the simulation was continued until a steady-state condition was reached.

The use of asynchronous motors (identified as M2, M3, M4, M5, M6, and M7) was hypothesized with, respectively, a 3.0 kW, 4.0 kW, 5.5 kW, 7.5 kW, 11 kW, and 15 kW electric power, to investigate the optimal connection between the horizontal centrifuge and the electric motor.

The motors were hypothesized to be driven by an electronic driver, i.e., an electronic VFD. The VFD measured efficiency was 0.95. The simulation concerned various cases, from an oversized IM to an overloaded IM, also testing various connections of the six motors and the horizontal centrifuge—varying the gearbox ratio for this reason—and between the electric line and the IMs using the VFD.

The parameters of the real motor (Table 2) and of the horizontal centrifuge (Table 3) were measured on the field and their values were inserted into the software simulation model, while, for the other IMs, their parameters were obtained from the datasheet by ABB.

The electric motor T-model equivalent circuit [18,19] was obtained from datasheets, considering the following standard tests:

- Motor running at no load;
- Motor running at rated load;
- Motor running at 145% of rated load (overloaded motor);
- Motor connected to the power line but with a locked rotor (i.e., short-circuit test).

Under the hypothesis that the rotor and stator inductances are equal [18], an iterative method has been developed and set, which, taking into account the four standard tests, as previously reported, and the measurements of voltage, current, speed, and torque, allows for the determination of the electrical parameters of the motor-equivalent T-model and,

in addition, the friction factor F. These parameters were subsequently entered into the Simulink simulation model.

Table 2. Electric three-phase induction motors M2, M3, M4, M5, M6, and M7, measured and calculated parameters to be inserted in Matlab's "Simulink" model.

	M2 (3.0 kW)	M3 (4.0 kW)	M4 (5.5 kW)	M5 (7.5 kW)	M6 (11 kW)	M7 (15 kW)
Electrical Active Power (kW)	3.5	4.7	6.4	8.6	12.4	16.6
Line Voltage (Vrms)	400	400	400	400	400	400
Line Current (Arms)	6.2	7.9	10.6	13.9	20.5	27.6
Frequency (Hz)	50	50	50	50	50	50
Power Factor	0.82	0.85	0.87	0.89	0.87	0.87
Poles Pairs	1	1	1	1	1	1
Efficiency	0.857	0.860	0.861	0.875	0.890	0.902
Mechanical Power (kW)	3.0	4.0	5.5	7.5	11.0	15.0
Torque (N.m)	9.86	13.24	18.45	25.04	36.32	49.36
Shaft RPM	2905	2885	2846	2860	2892	2902
Slip (%)	3.17	3.83	5.13	4.67	3.60	3.27
F (Friction Factor) (N.m.s)	2.43×10^{-4}	3.29×10^{-4}	4.65×10^{-4}	6.27×10^{-4}	9.01×10^{-4}	1.20×10^{-3}
J (Moment of Inertia) (kg.m^2)	0.0041	0.0061	0.014	0.016	0.038	0.048
Motor Type	Squirrel-cage	Squirrel-cage	Squirrel-cage	Squirrel-cage	Squirrel-cage	Squirrel-cage

Table 3. Horizontal centrifuge "Baby-1" measured and calculated parameters subsequently inserted in Matlab's "simulink" model.

Drum Operating Speed (rev/min)	Speed Variation	Gearbox Ratio	Gearbox Efficiency	Motor Shaft Operating Speed (rev/min)	Differential Scroll Speed (rev/min)	F (Friction Factor) (N·m·s)	J (Moment of Inertia) (kg·m^2)	Additional Torque When Loaded (N·m)
4916	Pulley with two toothed drive belts	1.7365	0.97	2831	12	0.009714	2.341	1.8025

To evaluate the amount of energy saving when the horizontal centrifuge is used in the olive oil mill, different connections of the VFD, IM, and horizontal centrifuge have been examined, varying the gearbox ratio from −45% up to +45% with reference to the measured nominal value of 1.7365.

The examined connection, for each motor, was the following:

- The VFD driving the IM with a closed-loop speed control, using V/Hz, slip regulation, and flux-oriented control by indirect field-oriented control;
- Speed change by varying the gearbox ratio (efficiency of 0.97) from −45% up to +45% with steps of 1%, a working IM speed set-point calculated from the gearbox ratio variation to reach 4916 rpm for the horizontal centrifuge working speed; the overall VFD and IM mechanical efficiency and the active electrical power sunk by the VFD and IM from the electric line was determined for each gearbox ratio step.

The field-oriented control algorithm or vector control algorithm [20,21], directly managing the V/Hz internal controller, changes and regulates the speed and torque of the IM; the regulator is based on the direct control of the IM current and voltage. When controlling an IM, this type of control is very common, due to its lower cost and its capability of regulating the motor speed more efficiently. Although this vector control algorithm can be operatively complicated to set up if compared to the simpler direct torque control, this algorithm does not need a frequent recalculation, thus requiring a lesser computational power than that required by the direct torque control algorithm [21]. The direct torque control algorithm is a method used by VFDs to regulate the speed and the torque of the IM, requiring the evaluation of the magnetic flux and torque based on the voltage and current

as measured for the IM, being a form of on/off control in the family of feedback control systems [22,23].

Moreover, the vector control algorithm allows for the enhanced dynamic behavior of the IM, allowing designers to optimally size the IM rather than oversize it to guarantee the desired transient behavior (i.e., a shorter time to reach the operational speed of the horizontal centrifuge). In addition, a smaller IM normally also delivers a larger fraction of its nominal power; thus, its operating point can offer a better overall efficiency [23].

Being interested in steady-state conditions, the horizontal centrifuge relation between rotational speed and loading torque needs to be carefully characterized. From Table 3, the horizontal centrifuge parameters are known, and, therefore, the mechanical system to be solved involves a general mechanical balance equation in order to calculate how the centrifuge speed depends on the applied torque. In addition, the gearbox ratio needs to be varied from −45% to +45% with reference to its nominal 1.7365 value.

The Simulink block that made this calculation possible is shown in Figure 1; Torque_in and epsilon_gear are the inputs while n_motor is the output. The decanter and induction motor are considered as an unicum and, for each single component, its friction factor (Fm) and its moment of inertia (Jm) are considered. The efficiency of the gearbox is eta_gear. The additional torque when the centrifuge is running loaded is considered through the LoadTorque input.

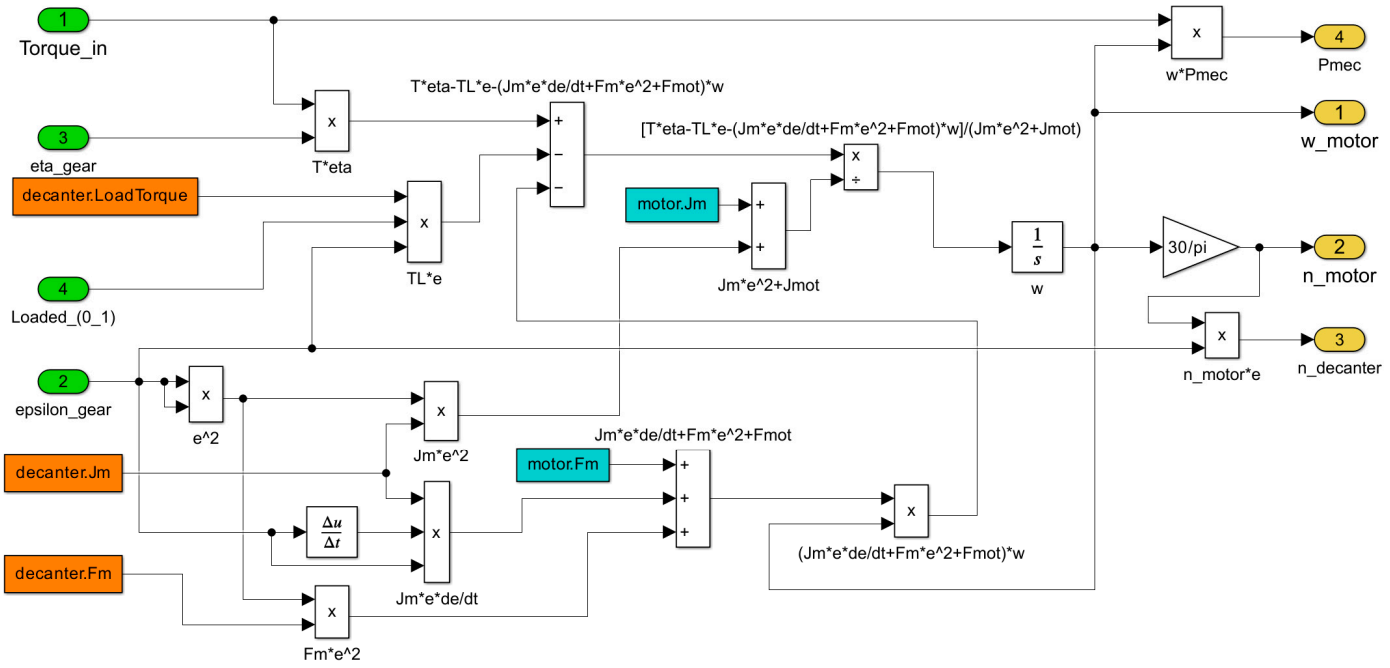

Figure 1. This Simulink block is utilized to solve the general mechanical balance of the horizontal decanter centrifuge and electric motor.

The parameterization consisted of stepping the torque (x-axis) from 0 N·m to 30 N·m with increments of 1 N·m and the gearbox percent ratio (y-axis) from −45% to +45% with increments of +1%, with reference to the nominal value of 1.7365, for each motor size and each decanter-loading condition. A long running time was required to perform the stepping process.

Subsequently, the collected data have been fitted using the Matlab 2024a Curve Fitter App, using a robust polynomial surface fit model with a first degree with reference to the x variable and a third degree with reference to the y variable (i.e., a poly13 surface fit model has been used, with seven coefficients, namely, f(x,y) = p00 + p10×x + p01×y + p11×x×y + p02×y^2 + p12×x×y^2 + p03×y^3), where the f(x,y) (i.e., the z-axis) represents the motor speed in rpm.

The obtained results are reported in Table 4, considering the M4 motor and the horizontal centrifuge not loaded.

Table 4. The polynomial surface fit model poly13 coefficients and their 95% confidence bounds when considering the M4 motor and the decanter not loaded.

Coefficient	Value	Lower 95% Confidence Bounds	Upper 95% Confidence Bounds
p00	−13.27	−21.36	−5.186
p10	548.6	548.1	549.1
p01	612.5	546.7	678.3
p11	−1109	−1111	−1106
p02	1736	1372	2101
p12	1487	1466	1508
p03	−27,486	−29,220	−25,750

The goodness of fit is very high, showing an adjusted coefficient of determination (R^2) of 1.0000, with a root mean square error (RMSE) of 23.1781. How much of the dependent variable can be predicted from the independent variables is shown by the R^2 value, which ranges from 0 to 1.

Finally, the simulated results, waiting until the system reached a steady-state condition, changing the electric motor size and with the horizontal centrifuge loaded and unloaded, were analyzed, using the Matlab R2024a and Simulink software. The simulations took a long time to complete.

3. Results

The primary parameter to be considered is the overall specific energy consumption (OSEC). The obtained simulation's results are depicted in Figure 2 and resumed in Table 5.

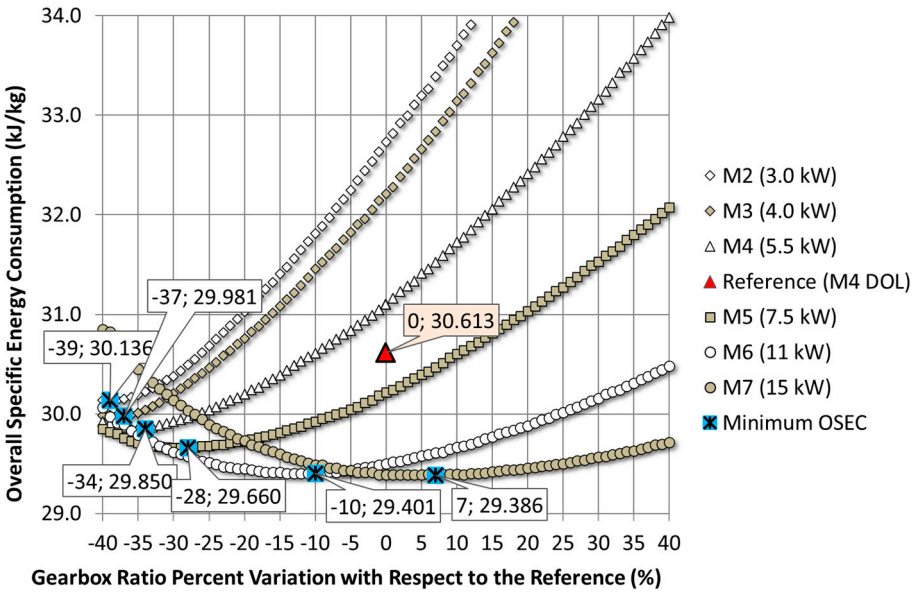

Figure 2. Simulink simulation results of the overall specific energy consumption (OSEC) versus the gearbox ratio percent variation, for each motor from M2 to M7.

Figure 2 shows the results of the simulations in terms of the overall specific energy consumption (OSEC) versus the gearbox ratio percent variation (GRPV), for each motor from M2 to M7. The decanter speed is controlled at 4916 rpm, although with a varying gearbox ratio. The minimum OSEC is achieved using the M7 motor at +7% GRPV, operating the M7 motor at a velocity of 2646 rpm.

Table 5. Simulink simulation results of the optimum overall specific energy consumption (OSEC) and the related overall process efficiency (OPE) at the optimum gearbox ratio percent variation that guarantees the minimum OSEC, for each motor from M2 to M7.

Motor Type	Motor Power (kW)	Minimum Overall Specific Energy Consumption (kJ/kg)	Overall Specific Energy Consumption Percent Saving Related to the Reference M4 DOL (%)	Optimum Gearbox Ratio Percent Variation (%)	Overall Process Efficiency	Decanter Speed (RPM)	Stator Current (A rms)
M2	3	30.136	1.56	−39	0.8172	4915.7	5.6
M3	4	29.981	2.06	−37	0.8214	4916.1	6.5
M4	5.5	29.850	2.49	−34	0.8249	4916.1	6.6
M5	7.5	29.660	3.11	−28	0.8302	4915.9	6.9
M6	11	29.401	3.96	−10	0.8375	4916.1	7.1
M7	15	29.386	4.01	+7	0.8380	4916.1	9.2

Furthermore, the graphs in Figure 2 show that the curves have a parabolic law behavior and that the motors are operated at a speed over 3000 rpm that corresponds to the synchronous speed of these three-phase motors (being f = 50 Hz and PolesPairs = 1, then the synchronous speed is 60×f/PolesPairs = 3000 rpm), except for the M7 motor, which is operated at 2646 rpm to reach its minimum OSEC and, therefore, below its synchronous speed.

Table 5 resumes the objective of this work: to determine when the OSEC reaches its minimum value and for which electric motor power and gearbox ratio value.

Table 5 also reports the minimum reached OSEC, showing the optimum GRPV and the operated electric motor. These values represent the minimum values as shown in Figure 2. In addition, the OSEC percent saving related to the reference (the M4 motor operated directly online) is reported in Table 5.

The decanter speed is controlled at 4916 rpm. The minimum OSEC is achieved by the M7 motor at +7% the optimum gearbox ratio percent variation; in this condition, the related energy saving resulted in +4.01% for the OSEC with reference to the M4 motor operated directly online (DOL).

In addition, Figure 3 shows the existing relation between the minimum OSEC and the electric motor nominal power. The data suggest the interpolation using a Gompertz sigmoid function as this function models very well the asymptotic behavior observed at 11 and 15 kW of motor power.

The Gompertz sigmoid function correlates very well (R^2 = 0.99427) and predicts what happens to the OSEC when using a motor with a different rated power; thanks to this, the equation can be considered very helpful. In addition, the equation suggests that, although the general behavior recommends that IM heavy oversizing can improve the process's overall energy saving, this should be compared to the asymptotic behavior of the equation itself.

In fact, at higher motor mechanical power values, an increment of the mechanical power brings a decrement of OSEC that can be unimportant if compared to the higher costs required to purchase both the IM and the VFD. This last consideration should be considered by adding it to the correlation equation of Figure 3: in this manner, an optimal minimum for the size of the IM could be obtained.

Moreover, to investigate the predictive capability of the results found, the OSEC curves have been modeled through a multiple linear regression, using as dependent variables the motor power (called x1) and GRPV (called x2). As the independent variable, or result variable, the OSEC (called y) was used.

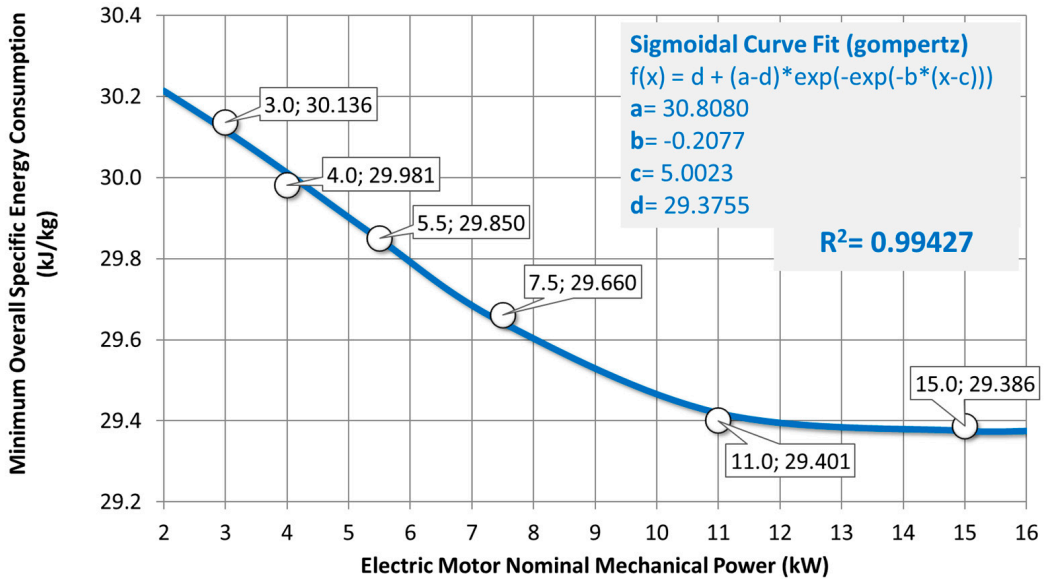

Figure 3. The minimum overall specific energy consumption (OSEC) versus the electric motor nominal mechanical power is related to a high degree of correlation (R^2 = 0.99427) to a Gompertz sigmoid function.

The interactions among the variables have been considered up to a degree of five: i.e., the considered multilinear model, when expressed in Wilkinson notation, was

y ~ 1 + x1^2 + x1×x2 + x2^2 + x1^3 + (x1^2):x2 + x1:(x2^2) + x2^3 + x1^4 + (x1^3):x2 + (x1^2):(x2^2) + x1:(x2^3) + x2^4 + x1^5 + (x1^4):x2 + (x1^3):(x2^2) + (x1^2):(x2^3) + x1:(x2^4) + x2^5

The model consists of 21 terms comprising the intercept term.

The normal algorithms used for the prediction assessment of multilinear models have been applied to this analysis. In particular, a 10-fold cross-validation using 500 Montecarlo runs was performed to assess the predictive performance of the model. The regression method used was principal component regression (PCR).

The multiple linear regression technique is used to statistically assess any existing relationship and to establish to what extent the model performs in the prediction of the property value; in our case, this corresponds to the confidence of the prediction of the OSEC value; the predicting capability must be quantified by a statistical point of view using techniques such as cross-validation (CV), involving the random partitioning of samples into complementary subsets such as the k-fold CV, or leave-one-out CV; these methods allow one to estimate the prediction capability of the model measured by the widespread ratio of the standard deviation of calibration data to the standard error of prediction data (RPD), as extensively described in the literature [24–28]. An RPD value greater than or equal to 5.0 indicates that the model is adequate for quality control, and a value greater than or equal to 8.1 indicates that the model is suitable to quantitatively measure the property of interest [25,29].

Subsequently, the ratio of the standard deviation of calibration data to the standard error of prediction data (RPD) was used to assess the prediction suitability; the RPD value was 37.21 ± 0.03 (that can be considered excellent), with a relative percent error in predicting the OSEC less than ±0.98% at 95% confidence bounds. These results guarantee the greater predictive confidence of the calculated model.

By analyzing the coefficient of variation of the model coefficients, it is possible to eliminate some interaction terms that decrease the model performance.

In fact, because the 10-fold CV gives ten estimates of the regression coefficient of each term, the identification of the problematic term could be performed considering the absolute value of the reciprocal of the coefficient of variation of the ten estimates of each

coefficient (INVCV) arising from the CV phase (i.e., the mean absolute value of the estimates of the regression coefficient divided by its standard deviation).

The minimum value of INVCV identifies the coefficient having the maximum estimated relative error (i.e., its coefficient of variation), and, therefore, it allows the identification of the interfering term that should be discarded on the next algorithm loop.

This method of "coefficient of variation algorithm" (CVA) has been successfully used in other research, showing excellent results [28,30]. The method allowed a reduction of the terms considered in the model.

The model was reduced to 16 terms, comprising the intercept term. Its expression, in Wilkinson notation, is

y ~ 1 + x1 + x2 + x1^2 + x1:x2 + x2^2 + x1^3 + (x1^2):x2 + x1:(x2^2) + x1^4 + (x1^3):x2 + (x1^2):(x2^2) + x2^4 + x1^5 + (x1^4):x2 + x2^5

In Figure 4, the contour plots of the found model calculated over the span of motor powers and GRPV values are reported.

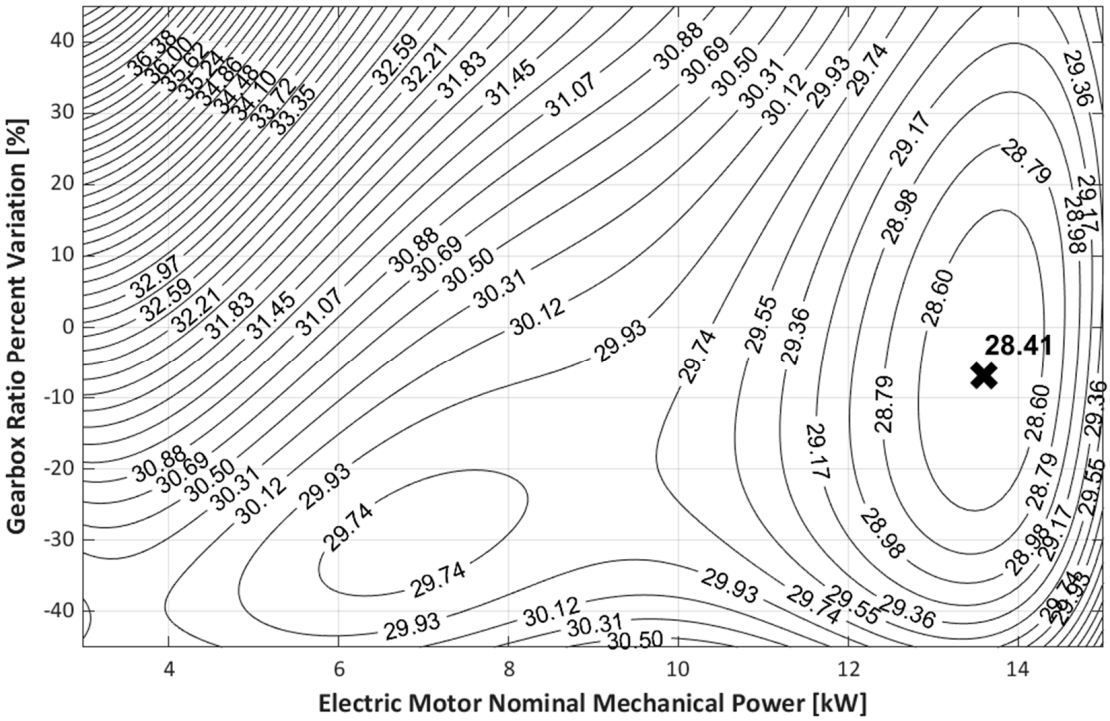

Figure 4. OSEC values (kJ/kg) contour plots of the found multilinear model calculated over the span of motor powers and GRPV values. The cross marker indicates the minimum value of OSEC.

Figure 4 shows the existence of a minimum OSEC of 28.41 kJ/kg, located at GRPV= −6.8%, and a motor power of 13.6 kW. It has to be highlighted that Figure 3 does not show the existence of this minimum.

Figures 5 and 6 show the further steps taken into account to successfully close the minimization step.

From a survey market of the currently available IMs and VFDs, the trend of their cost has been calculated, as depicted in Figure 5. The trend line is hypothesized to be a power law equation.

Moreover, hypothesizing that the cost of the IM + VFD is spread over ten campaigns, and that the overall processed product is 226,685 kg for each campaign (627 overall working hours), then the related incidence of machines cost per kg of processed product can be calculated.

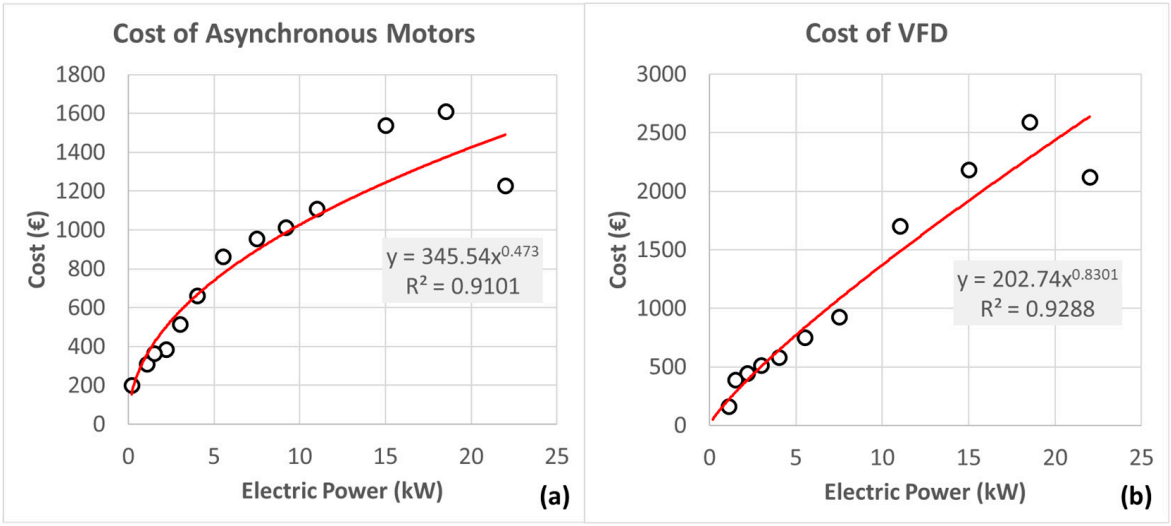

Figure 5. Survey market of IMs and VFDs. (**a**) Cost of asynchronous motors. (**b**) Cost of VFDs. The trend line is hypothesized to be a power law one.

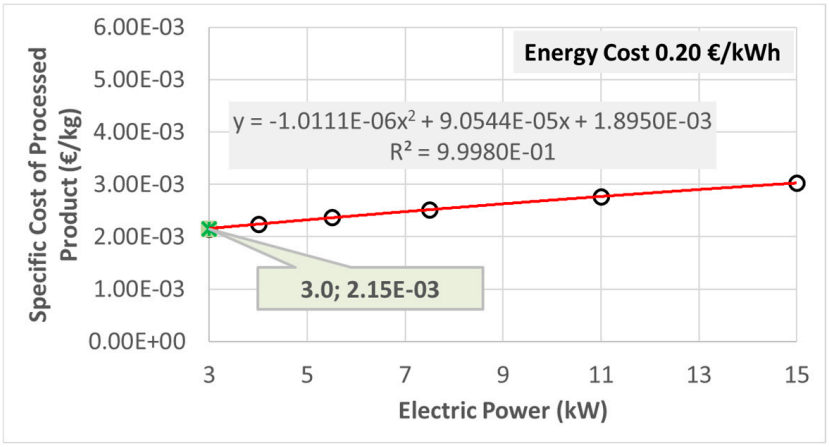

Figure 6. Sum of machines cost and specific cost due to process per each kg of processed product versus size of induction motor and variable frequency driver used. The energy cost is assumed to be 0.20 EUR/kWh.

The cost related to the OSEC is obtained considering an energy cost of 0.20 EUR/kWh (the average price for medium-sized consumers in the EU in the second half of 2023, according to Eurostat). Thus, the data of Table 5 can be transformed into the specific cost due to the process per kg of processed product (SCOPP).

The sum of these two costs brings the data shown in Figure 6 representing the classical curve that allows the minimization of costs.

Figure 6 shows the sum between the machines' cost (IM + VFD on ten campaigns) and the specific cost due to the process per kg of processed product versus the size of the IM and VFD used. The interpolating curve is hypothesized to be a parabolic law; this hypothesis allows us to straightforwardly obtain the minimum of the curve.

The predicted optimum size of the IM + VFD (the minimum of the curve) to be used results in 3.0 kW (the minimum tested motor), this being far from the size of the motor currently used on the real machine (5.5 kW).

This is mainly due to the low cost of electric energy when compared with the purchase of the machines. However, the time required to bring the decanter up to the rated speed must also be taken into account. In addition, the specific energy consumption depends on the mill size. The reduction in specific energy consumption will depend both on the treated

product and on the efficiency of the machines. Overall, therefore, the cost will depend on the energy cost and devices cost.

Therefore, even if Figure 4 indicates a minimum OSEC of 28.41 kJ/kg, located at GRPV= −6.8% and a motor power of 13.6 kW, when transformed to the cost level, this minimum moves, due to machines cost entering into the calculation, thus bringing one to a less convenient minimum from the energetic point of view but one that is economically more convenient.

To complete the discussion of the problem, it is necessary to obtain what was calculated in Figure 6 using the model determined in Figure 4, in order to obtain the SCOPP as a surface over the span of motor powers and GRPV values.

Figure 7 shows, using the previously calculated model, as shown in Figure 4, the sum between the machines' cost (IM + VFD on ten campaigns) and the specific cost due to the process per kg of processed product versus the size of IM and VFD used, and the GRPV variation.

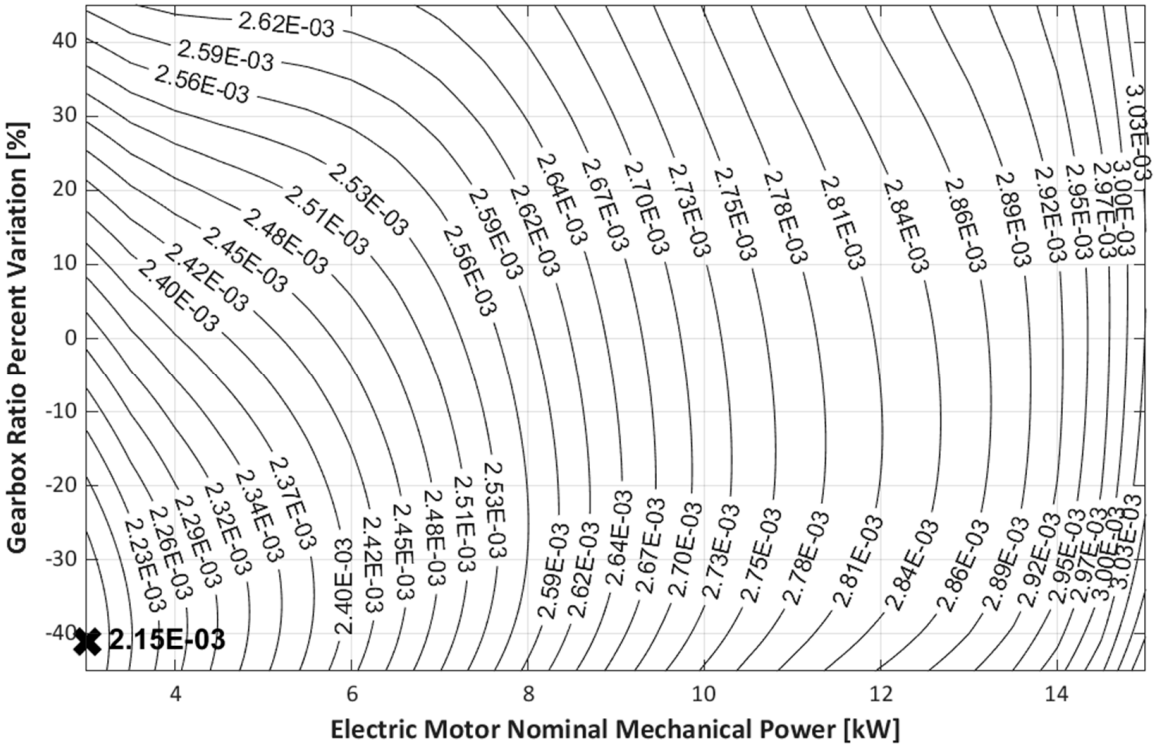

Figure 7. SCOPP value (EUR/kg) contour plots of the found multilinear model calculated over the span of motor powers and GRPV values. The energy cost is assumed to be 0.20 EUR/kWh. The cross marker indicates the minimum value of SCOPP.

The predicted optimum size of IM + VFD (the minimum value on the surface of Figure 7) to be used results in 3.0 kW (corresponding to the minimum tested motor) with a GRPV of −41%, being far from the size of the motor currently used on the real machine (5.5 kW). It should be highlighted that Table 5 predicted a GRPV of −39%, while Figure 6 predicted a SCOPP of 2.22×10^{-3}.

The results are approximately the same, but Figure 7 is more accurate.

Moreover, Figure 7 shows that from the point of view of the SCOPP, motors with lower power are convenient to run at high speed (negative value of GRPV) while the opposite must be done with higher-power motors (positive GRPV).

4. Conclusions

In this work, the analysis and modeling of the optimal connection between different IMs and a horizontal decanter centrifuge used in olive oil extraction, using different gearbox ratios, and between a driving electronic VFD and different IMs, were examined.

The simulation helped to test the system by simulation, avoiding the elevated costs needed for the purchase of motors and variable-frequency drivers.

The trials showed that to improve the efficiency of the overall process and to decrease the overall specific energy consumption, motor oversizing is mandatory. The results show that, in our case, an overall specific energy consumption percent saving of 3.1% and 4.0% can be achieved, with a slight (7.5 kW) and a medium (11 kW) oversizing of the induction motor, respectively.

However, the asymptotic behavior of the specific energy consumption, being related to the motor power, places an economic limit on the motor oversizing.

In fact, at higher motor mechanical power values, a mechanical power increment brings an overall specific energy consumption decrement that, however, can be unimportant if compared to the higher costs required to purchase both the electrical motor and the variable frequency driver; this last condition must be added into the relation existing between the overall specific energy consumption and electric motor rated mechanical power, to build the minimization equation allowing for the optimal selection of motor size. The predicted optimum size of IM + VFD to be used resulted in 3.0 kW, this being far from the size of the motor currently used on the real machine (5.5 kW). However, the time required to bring the decanter up to the rated speed must also be taken into account. Moreover, the specific energy consumption depends on the mill size. The reduction in specific energy consumption will depend both on the treated product and on the efficiency of the machines. Overall, therefore, the cost will depend on the energy cost and devices cost.

The methodology has led to consistent results; however, further investigation is needed to properly evaluate a suitable method for IM oversizing and to estimate the reliability of the model prediction when it is extended to a larger industrial decanter.

Author Contributions: Conceptualization, G.A., O.M. and G.C.D.R.; methodology, S.L. and M.R.; software, G.A.; validation, O.M., F.G., M.R. and A.M.; formal analysis, A.M., M.R. and F.G.; investigation, L.S., A.M. and F.G.; resources, L.S. and M.R.; data curation, S.L. and M.R.; writing—original draft preparation, G.A. and O.M.; writing—review and editing, G.A. and O.M.; visualization, L.S.; supervision, G.C.D.R.; project administration, G.A. and F.G.; funding acquisition, G.C.D.R. All authors have read and agreed to the published version of the manuscript.

Funding: This study was carried out within the Agritech National Research Center and received funding from the European Union Next Generation EU (PIANO NAZIONALE DI RIPRESA E RESILIENZA (PNRR)—MISSIONE 4 COMPONENTE 2, INVESTIMENTO 1.4—D.D. 1032 17/06/2022, CN00000022). This manuscript reflects only the authors' views and opinions; neither the European Union nor the European Commission can be considered responsible for them.

Institutional Review Board Statement: Not applicable.

Informed Consent Statement: Not applicable.

Data Availability Statement: The raw data supporting the conclusions of this article will be made available by the correspondence author on request.

Conflicts of Interest: The authors declare no conflicts of interest.

References

1. Lu, S.-M. A Review of High-Efficiency Motors: Specification, Policy, and Technology. *Renew. Sustain. Energy Rev.* **2016**, *59*, 1–12. [CrossRef]
2. Bertoldi, P. (Ed.) *Energy Efficiency in Motor Systems*; Springer Proceedings in Energy; Springer International Publishing: Cham, Switzerland, 2021; ISBN 978-3-030-69798-3.

3. Al-Quraan, T.M.A.; Vovk, O.; Halko, S.; Kvitka, S.; Suprun, O.; Miroshnyk, O.; Nitsenko, V.; Zayed, N.M.; Islam, K.M.A. Energy-Saving Load Control of Induction Electric Motors for Drives of Working Machines to Reduce Thermal Wear. *Inventions* **2022**, *7*, 92. [CrossRef]
4. Trianni, A.; Cagno, E.; Accordini, D. Energy Efficiency Measures in Electric Motors Systems: A Novel Classification Highlighting Specific Implications in Their Adoption. *Appl. Energy* **2019**, *252*, 113481. [CrossRef]
5. Aree, P. Condition for Maximum Efficiency of Three-Phase Induction Motors. In Proceedings of the 2022 19th International Conference on Electrical Engineering/Electronics, Computer, Telecommunications and Information Technology (ECTI-CON), Prachuap Khiri Khan, Thailand, 24 May 2022; IEEE: Piscataway, NJ, USA, 2022; pp. 1–4.
6. Abbott, L., III. Power Quality and Cost Analysis of Industrial Electrical Distribution Systems with Adjustable Speed Drives. Master's Thesis, California State University, Long Beach, CA, USA, 2006.
7. Saidur, R.; Mekhilef, S.; Ali, M.B.; Safari, A.; Mohammed, H.A. Applications of Variable Speed Drive (VSD) in Electrical Motors Energy Savings. *Renew. Sustain. Energy Rev.* **2012**, *16*, 543–550. [CrossRef]
8. Wang, G.; Song, L. Performance Assessment of Variable Frequency Drives in Heating, Ventilation, and Air-Conditioning Systems. *Sci. Technol. Built Environ.* **2018**, *24*, 1075–1083. [CrossRef]
9. Ekren, O.; Celik, S.; Noble, B.; Krauss, R. Performance Evaluation of a Variable Speed DC Compressor. *Int. J. Refrig.* **2013**, *36*, 745–757. [CrossRef]
10. Piedrahita-Velásquez, C.A.; Ciro-Velásquez, H.J.; Gómez-Botero, M.A. Identification and Digital Control of a Household Refrigeration System with a Variable Speed Compressor. *Int. J. Refrig.* **2014**, *48*, 178–187. [CrossRef]
11. Yilmaz, O.; Bayar, H.; Başhan, V.; Yigit, K. Experimental Energy and Exergy Analyses of Ship Refrigeration System Operated by Frequency Inverter at Varying Sea Water Temperatures. *J. Braz. Soc. Mech. Sci. Eng.* **2022**, *44*, 133. [CrossRef]
12. Cini, E.; Recchia, L.; Daou, M.; Boncinelli, P. Human Health Benefits and Energy Saving in Olive Oil Mills. In Proceedings of the International Conference, Innovation Technology to Empower Safety, Health and Welfare in Agriculture and Agro-Food Systems, Ragusa Safety Health Welfare, Ragusa, Italy, 15–17 September 2008.
13. Tamborrino, A.; Perone, C.; Catalano, F.; Squeo, G.; Caponio, F.; Bianchi, B. Modelling Energy Consumption and Energy-Saving in High-Quality Olive Oil Decanter Centrifuge: Numerical Study and Experimental Validation. *Energy* **2019**, *12*, 2592. [CrossRef]
14. Leone, A.; Perone, C.; Berardi, A.; Tamborrino, A. Energy Analysis and Numerical Evaluation of the Decanter Centrifuge for Wastewater Management to Allow a Sustainable Energy Planning of the Process. *Energy Convers. Manag. X* **2024**, *22*, 100596. [CrossRef]
15. Latchoomun, L.; Gokhool, C.; Ah King, R.T.F.; Busawon, K.; Barbot, J.P. Efficiency of VFD Coupled Induction Motors Operating in the Scalar Mode with Different Types of Loads. In *Smart and Sustainable Engineering for Next Generation Applications: Proceeding of the Second International Conference on Emerging Trends in Electrical, Electronic and Communications Engineering (ELECOM 2018), 28–30 November 2018*; Springer: Berlin/Heidelberg, Germany, 2019; pp. 45–59.
16. Zakharov, A.V. Software Simulation and Analysis of Transient Processes in Engineering Problems of Induction-Motor Design. *Russ. Electr. Eng.* **2008**, *79*, 174–177. [CrossRef]
17. Krenicky, T.; Nikitin, Y.; Božek, P. Model-Based Design of Induction Motor Control System in MATLAB. *Appl. Sci.* **2022**, *12*, 11957. [CrossRef]
18. Davey, K.R. The Equivalent T Circuit of the Induction Motor: Its Nonuniqueness and Use to the Magnetic Field Analyst. In Proceedings of the 12th Biennial IEEE Conference on Electromagnetic Field Computation, CEFC 2006, Miami, FL, USA, 30 April–3 May 2006; p. 175. [CrossRef]
19. Khoury, G.; Ghosn, R.; Khatounian, F.; Fadel, M.; Tientcheu, M. Including Core Losses in Induction Motors Dynamic Model. In Proceedings of the 2016 3rd International Conference on Renewable Energies for Developing Countries, REDEC 2016, Zouk Mosbeh, Lebanon, 13–15 July 2016; pp. 1–6. [CrossRef]
20. Stopa, P. High Speed Field Oriented Control. Master's Thesis, Aalborg University, Aalborg, Denmark, 2009.
21. Wang, F.; Zhang, Z.; Mei, X.; Rodríguez, J.; Kennel, R. Advanced Control Strategies of Induction Machine: Field Oriented Control, Direct Torque Control and Model Predictive Control. *Energy* **2018**, *11*, 120. [CrossRef]
22. Lai, Y.-S.; Chen, J.-H. A New Approach to Direct Torque Control of Induction Motor Drives for Constant Inverter Switching Frequency and Torque Ripple Reduction. *IEEE Trans. Energy Convers.* **2001**, *16*, 220–227. [CrossRef]
23. Casadei, D.; Profumo, F.; Serra, G.; Tani, A. FOC and DTC: Two Viable Schemes for Induction Motors Torque Control. *IEEE Trans. Power Electron.* **2002**, *17*, 779–787. [CrossRef]
24. Porep, J.U.; Kammerer, D.R.; Carle, R. On-Line Application of near Infrared (NIR) Spectroscopy in Food Production. *Trends Food Sci. Technol.* **2015**, *46*, 211–230. [CrossRef]
25. Kays, S.E.; Archibald, D.D.; Sohn, M. Prediction of Fat in Intact Cereal Food Products Using Near-Infrared Reflectance Spectroscopy. *J. Sci. Food Agric.* **2005**, *85*, 1596–1602. [CrossRef]
26. Nicolaï, B.M.; Beullens, K.; Bobelyn, E.; Peirs, A.; Saeys, W.; Theron, K.I.; Lammertyn, J. Nondestructive Measurement of Fruit and Vegetable Quality by Means of NIR Spectroscopy: A Review. *Postharvest Biol. Technol.* **2007**, *46*, 99–118. [CrossRef]
27. Picard, R.R.; Cook, R.D. Cross-Validation of Regression Models. *J. Am. Stat. Assoc.* **1984**, *79*, 575–583. [CrossRef]
28. Altieri, G.; Genovese, F.; Tauriello, A.; Di Renzo, G.C. Models to Improve the Non-Destructive Analysis of Persimmon Fruit Properties by VIS/NIR Spectrometry. *J. Sci. Food Agric.* **2017**, *97*, 5302–5310. [CrossRef]

29. Esteve Agelet, L.; Armstrong, P.R.; Romagosa Clariana, I.; Hurburgh, C.R. Measurement of Single Soybean Seed Attributes by Near-Infrared Technologies. A Comparative Study. *J. Agric. Food Chem.* **2012**, *60*, 8314–8322. [CrossRef] [PubMed]
30. Altieri, G.; Matera, A.; Genovese, F.; Di Renzo, G.C. Models for the Rapid Assessment of Water and Oil Content in Olive Pomace by Near-Infrared Spectrometry. *J. Sci. Food Agric.* **2020**, *100*, 3236–3245. [CrossRef] [PubMed]